Journal of Non-Crystalline Solids 459 (2017) 130–141

Contents lists available at ScienceDirect

Journal of Non-Crystalline Solids

journal homepage: www.elsevier.com/locate/jnoncrysol

Serrated flow of CuZr-based bulk metallic glasses probed by nanoindentation: Role of the activation barrier, size and distribution of shear transformation zones

R. Limbach [a], K. Kosiba [b], S. Pauly [b], U. Kühn [b], L. Wondraczek [a,*]

[a] Otto Schott Institute of Materials Research, University of Jena, Fraunhoferstraße 6, 07743 Jena, Germany
[b] Institute for Complex Materials, IFW Dresden, Helmholtzstraße 20, 01069 Dresden, Germany

ARTICLE INFO

Article history:
Received 28 November 2016
Received in revised form 3 January 2017
Accepted 4 January 2017
Available online 18 January 2017

Keywords:
Metallic glass
Nanoindentation
Strain-rate sensitivity
Shear transformation zone

ABSTRACT

We report on the effect of Al and Co alloying in vitreous $Cu_{50}Zr_{50}$ on local deformation and serrated flow as a model for relating the size and localization of shear transformation zones (STZ) to Poisson ratio and strain-rate sensitivity of metallic glasses. Alloying with Al results in significant variations in mechanical performance, in particular, in Young's modulus, hardness and strain-rate sensitivity. Increasing strain-rate sensitivity with increasing degree of alloying indicates a reduced tendency for shear localization. In parallel, a gradual transition from inhomogeneous to homogeneous plastic flow is observed. Using a statistical analysis of the shear stress associated with the initiation of the first pop-in in the load-displacement curve during spherical indentation, the activation volume for plastic flow at the onset of yielding is reported. This analysis is employed for experimental evaluation of the compositional dependence of activation barrier, size and distribution of STZs. It is demonstrated that the STZ size does not change significantly upon Al alloying and encompasses a local volume of around 22–24 atoms. However, the barrier energy density for the initiation of a single STZ progressively increases. The broader distribution of STZs impedes their accumulation into larger-size flow units, leading to a lower number and reduced size of serrations in the load-displacement curve. On the contrary, lower barrier energy densities enable a larger quantity of STZs to be activated simultaneously. These STZs can easily percolate into large flow units, promoting plastic flow through their interaction. We employ Poisson's ratio as an indicator for plasticity to shown that this interpretation can be transferred to other types of metallic glasses. That is, larger flow units were found for metallic glasses with higher Poisson ratio and more pronounced plasticity, while the flow units in alloys with very low Poisson ratio and high brittleness are significantly reduced in size and more homogeneously distributed throughout the material.

1. Introduction

Since their first discovery, metallic glasses have received considerable attention. This has been due to their assumed potential for application as structural material [1]. Compared to their polycrystalline counterparts, metallic glasses exhibit a disordered structure of densely packed atomic clusters with predominantly metallic bonding character [2–4]. This atomic configuration and, in particular, the absence of long-range order result in an interesting set of mechanical properties, i.e., typically high elastic limit, exceptional strength and hardness or strong abrasion wear resistance [1]. However, actual use of metallic glasses is still restricted to niche applications, a fact that originates mainly from limitations in their processing as well as the lack of ductility [5]. To address these issues, research has been focusing on the technical exploitation of new alloys with improved glass-forming ability [6,7], and on the understanding of fundamental deformation processes and their consequences for macroscopic mechanical behavior [4,8–11].

In the present understanding, the deformation of metallic glasses is generally thought to be determined by a cooperative rearrangement of a group of atoms [12], termed *shear transformation zone* (STZ) [13]. A STZ typically comprises a volume of up to about 100 atoms, and is preferentially formed around regions of high free volume [8]. However, as opposed to structural defects in crystalline materials (such as dislocations), a STZ is a transient state induced through externally applied stress and, hence, the operation of a STZ can effectively be identified only from differences in the atomic configuration before or after deformation [4]. Experimental evaluation of the shape, size or activation energy of a STZ is difficult, and most of the present understanding is obtained from computational simulation. However, over the past years, various protocols have been proposed also for the experimental observation of STZs. For example, Choi et al. [14] estimated the

* Corresponding author.
E-mail address: lothar.wondraczek@uni-jena.de (L. Wondraczek).

http://dx.doi.org/10.1016/j.jnoncrysol.2017.01.015

activation volume of a single STZ from a statistical analysis of the maximum shear stress associated with the initiation of the first discontinuity, or "pop-in", in the load-displacement curve of a nanoindentation experiment. Pan et al. [15] utilized a nanoindentation set-up with strain-rate jumps and derived the STZ volume from the strain-rate sensitivity. In both approaches, the STZ volume was calculated following the cooperative shear model of Johnson and Samwer [16]. Results obtained in these preliminary investigations were found to be in good agreement with those from other reports. Subsequent studies tried to establish fundamental correlations between the STZ size and other physical properties, such as the glass-transition temperature [17–19], elastic modulus [20] or toughness [15,21]. It was found that the STZ size seems to be strongly related to the atomic configuration in the metallic glass, i.e., order on short and intermediate length scale, as well as on the amount and local distribution of free volume [18,22–26]. On the other hand, most studies performed so far did focus on the comparison of very different alloy systems, ranging from Pt-, Pd-, Co- and W-based metallic glasses and metalloid-free alloys with Cu, Ni or Zr as the host element to compositions based on La [15,17,19,21,27]. Information on the influence of minor compositional variations on the STZ size in a specific alloy system are relatively sparse [20,24,28]. In particular, although the initiation of a STZ is supposed to be the fundamental process in the strong localization of plastic flow in metallic glasses via the operation of individual shear bands, to our knowledge, no studies have investigated the relationship between the STZ size and the shear band formation upon indentation in a systematic series of interrelated glass-forming alloys.

For that reason, we studied the indentation response of metallic glasses in the well-known ternary Cu-Zr-Al. With the addition of Al to binary $Cu_{50}Zr_{50}$ alloys, not only the glass-forming ability significantly increases [29–34], but also the mechanical properties are known to change notably (for example, room-temperature plasticity [33–36] or elastic modulus [33,35,36]). We now relate these changes to changes in strain-rate sensitivity and serrated flow behavior. In addition to Al, we further consider the impact of alloying with Co. The activation volume of STZs is then determined using a statistical analysis of the maximum shear stress at the initiation of the first pop-in [14], as well as through the nanoindentation strain-rate jump test [37]. Finally, correlations are drawn between the STZ size and the plastic flow of ternary $(Cu_{0.5}Zr_{0.5})_{100-x}Al_x$ and quaternary $Cu_{46-y}Zr_{46}Al_8Co_y$ (y = 1 and 2 at.%) alloys.

2. Materials and methods

Precursor alloys with nominal compositions of $(Cu_{0.5}Zr_{0.5})_{100-x}Al_x$ (x = 4, 5, 6, 7 and 8 at.%), $Cu_{46-y}Zr_{46}Al_8Co_y$ (y = 1 and 2 at.%) and $Zr_{52.5}Cu_{17.9}Ni_{14.6}Al_{10}Ti_5$ (as a reference material) were obtained by mixing high-purity elements (≥99.99%) in a Ti-gettered Ar atmosphere using an arc melter (Edmund Bühler GmbH). The ingots were remelted three times in order to ensure chemical homogeneity. From the ingots, cylindrical rods with a length of 35 mm and a diameter of 2 mm were prepared by suction casting inside the arc melter. The structure of the specimen was investigated by means of X-ray diffraction in a STOE STADI P diffractometer (STOE & Cie GmbH) using $MoK_{\alpha1}$ radiation and operating in transmission mode. A Perkin-Elmer differential scanning calorimeter (Diamond DSC, PerkinElmer Inc.) was employed to determine the glass-transition temperature, T_g, and the onset of crystallization, T_x, at a heating rate of 40 K/min.

The mechanical properties were investigated by instrumented indentation testing, using a nanoindenter (G200, Agilent Inc.). For this purpose, samples of about 1.5 mm in height were taken from the bottom end of the cylindrical rods and polished in both ends. Depth profiles of the modulus, E, and hardness, H, were obtained through constant strain-rate indentations conducted in the continuous stiffness measurement mode [37]. In this setup, a weak oscillation (Δh = 2 nm, f = 45 Hz) is applied to the three-sided Berkovich diamond tip used for indentation (Synton-MDP Inc.), which enables the simultaneous determination of E and H as a function of the indenter displacement. On every sample, at least 15 indents with a maximum depth of 2 μm were created at a strain-rate of 0.05 s^{-1}.

Additionally, a nanoindentation strain-rate jump test [37], was performed to study the indentation creep behavior. In this test, the Berkovich indenter tip initially penetrates the sample surface to a depth of 800 nm at a constant strain-rate of 0.05 s^{-1}. Subsequently, the strain-rate was changed across intervals of 200 nm. The resulting variation of the hardness was determined using the continuous stiffness measurement mode (Δh = 5 nm, f = 45 Hz). Ten strain-rate jump tests with strain-rates of 0.014, 0.004 and 0.001 s^{-1} (in a descending order) were performed on each sample.

The rate-dependence of the indentation deformation was further studied using a conical diamond indenter tip (SURFACE Systems & Technology GmbH & Co. KG) with a tip-angle of 60° and an effective radius of 4.53 μm. Indents with a peak load of 50 mN were created at varying loading rates, ranging from around 0.033 up to 10 mN/s, and the resulting load-displacement curves were recorded with data acquisition rates of up to 500 Hz. The dwell-time at maximum load was kept constant at 5 s.

The tip area function of both the Berkovich and conical diamond tips as well as the instrument's frame compliance were calibrated prior to the measurements on a fused silica reference glass sample (Corning code 7980, Corning Inc.), according to the method introduced by Oliver and Pharr [38]. To avoid the influence of residual stress fields, consecutive indents were conducted at distances of 30 μm (conical tip) and 50 μm (Berkovich tip), respectively [39]. All experiments were performed in laboratory air under ambient conditions at temperatures of around (30 ± 2) °C and with thermal drift rates of <0.05 nm/s.

3. Results and discussion

3.1. Glass formation and thermal stability

The X-ray diffraction patterns of the ternary $(Cu_{0.5}Zr_{0.5})_{100-x}Al_x$ (x = 4, 5, 6, 7 and 8 at.%) and the quaternary $Cu_{46-y}Zr_{46}Al_8Co_y$ (y = 1 and 2 at.%) alloys are presented in Fig. 1. All samples exhibit a characteristic broad diffraction maximum with no evidence of crystallinity. This finding is also supported by the results from the thermal analysis shown in Fig. 2 and summarized in Table 1. With increasing temperature, a weak endothermic event corresponding to the glass-transition is seen in all samples. This is followed by a supercooled liquid region, and a single sharp exothermic peak, indicating crystallization. Regarding the ternary $(Cu_{0.5}Zr_{0.5})_{100-x}Al_x$, the values of T_g and T_x increase with increasing Al content, i.e., from T_g = 691 ± 2 K and T_x = 754 ± 2 K ($Cu_{48}Zr_{48}Al_4$) up to T_g = 711 ± 2 K and T_x = 794 ± 2 K ($Cu_{46}Zr_{46}Al_8$), respectively. Furthermore, the incorporation of additional Al results in an expansion of the supercooled liquid region, $\Delta T = T_x - T_g$, by about 19 K ($Cu_{48}Zr_{48}Al_4$: ΔT = 63 ± 2 K and $Cu_{46}Zr_{46}Al_8$: ΔT = 82 ± 2 K), indicating an increased stability of the supercooled liquid against crystallization and an associated increase of glass-forming ability [6]. Both these compositional trends as well as the absolute values of T_g, T_x and ΔT of these glasses agree very well with previous investigations [29–34]. The enhanced thermal stability of Al-containing $Cu_{50}Zr_{50}$ alloys has been assigned to the significant size mismatch among the densely packed Cu (0.135 nm), Zr (0.155 nm) and Al (0.125 nm) atoms on the one hand [6,40,41]. On the other hand, the larger negative enthalpy of mixing between Al and Zr (−44 kJ/mol) compared to Al and Cu (−1 kJ/mol) or Cu and Zr (−23 kJ/mol) is supposed to counteract the crystallization of ternary Cu-Zr-Al alloys during cooling [29,42]. In contrast to the effect of Al, the addition of small amounts of Co seems to have only negligible impact on the glass-forming ability of the $Cu_{46}Zr_{46}Al_8$ alloy, as the values of T_g, T_x as well as ΔT remain almost unchanged within the limits of experimental error.

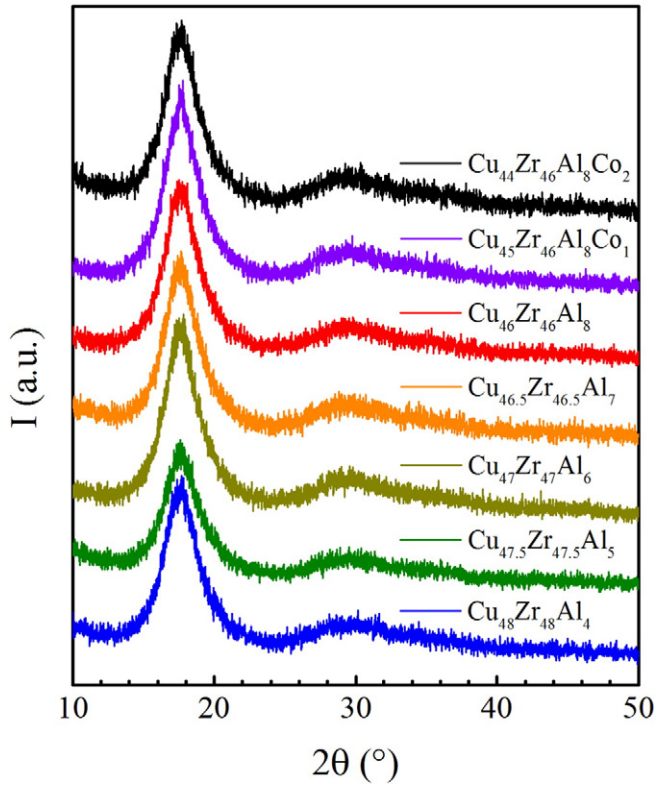

Fig. 1. X-ray diffraction patterns of the ternary $(Cu_{0.5}Zr_{0.5})_{100-x}Al_x$ (x = 4, 5, 6, 7 and 8 at.%) and quaternary $Cu_{46-y}Zr_{46}Al_8Co_y$ (y = 1 and 2 at.%) alloys.

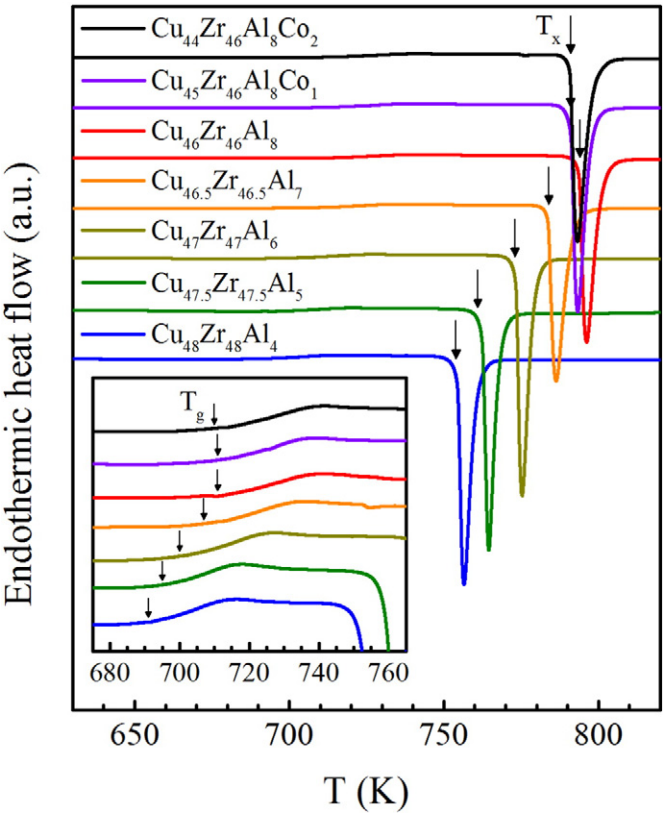

Fig. 2. DSC curves of the ternary $(Cu_{0.5}Zr_{0.5})_{100-x}Al_x$ (x = 4, 5, 6, 7 and 8 at.%) and quaternary $Cu_{46-y}Zr_{46}Al_8Co_y$ (y = 1 and 2 at.%) alloys. The arrows mark the onsets of the glass-transition temperature, T_g, and of crystallization, T_x, respectively.

Table 1
Thermal and mechanical properties of ternary $(Cu_{0.5}Zr_{0.5})_{100-x}Al_x$ (x = 4, 5, 6, 7 and 8 at.%) and quaternary $Cu_{46-y}Zr_{46}Al_8Co_y$ (y = 1 and 2 at.%) vitreous alloys. The glass-transition temperature, T_g, onset of crystallization, T_x and supercooled liquid region, $\Delta T = T_x - T_g$, were determined by differential scanning calorimetry (DSC). The modulus, E, hardness, H, and strain-rate sensitivity, m, were characterized through depth-resolved indentation testing. Experimental results for glassy $Zr_{52.5}Cu_{17.9}Ni_{14.6}Al_{10}Ti_5$ are added for comparison.

Composition (at.%)	T_g (K)	T_x (K)	ΔT (K)	E (GPa)[a]	H (GPa)[a]	m
$Cu_{48}Zr_{48}Al_4$	691	754	63	113.6	6.94	0.0056
$Cu_{47.5}Zr_{47.5}Al_5$	695	761	66	113.8	7.07	0.0081
$Cu_{47}Zr_{47}Al_6$	700	773	73	116.2	7.27	0.0109
$Cu_{46.5}Zr_{46.5}Al_7$	707	784	77	118.9	7.43	0.0116
$Cu_{46}Zr_{46}Al_8$	711	794	82	120.4	7.60	0.0130
$Cu_{45}Zr_{46}Al_8Co_1$	711	791	80	122.4	7.67	0.0138
$Cu_{44}Zr_{46}Al_8Co_2$	710	791	81	122.1	7.51	0.0115
$Zr_{52.5}Cu_{17.9}Ni_{14.6}Al_{10}Ti_5$	677[b]	738[b]	61[b]	112.7	6.48	0.0086
Experimental error	±2	±2	±4	±0.8	±0.06	n.a.[c]

[a] Values of E and H were averaged between the upper 10% and lower 20% of each indentation depth profile.
[b] Experimental results on T_g, T_x and ΔT were taken from Ref. [83].
[c] For each alloy, a correlation factor, R^2, higher than 0.99 was achieved in the linear regression.

3.2. Size and rate dependence of the mechanical properties

Further characterization of the ternary Cu-Zr-Al and quaternary Cu-Zr-Al-Co alloys was conducted through depth-resolved indentation testing. Results on the modulus, E, hardness, H and strain-rate sensitivity, m, are summarized in Table 1. Constant strain-rate indentations were performed to evaluate the effect of the Al and Co alloying on the modulus and hardness within the two alloy series. Depth profiles of the modulus and hardness obtained in that way are exemplarily shown for a $Cu_{48}Zr_{48}Al_4$ alloy in the Fig. 3a and b. The hardness was determined from the load, P, divided by the projected contact area of the indenter tip, A_c [38]:

$$H = \frac{P}{A_c} \tag{1}$$

The modulus was derived from the reduced elastic modulus, E_r, which reflects the combined elastic response of the indenter tip and the glass specimen [38],

$$E_r = \left[\frac{(1-\nu_i^2)}{E_i} + \frac{(1-\nu_s^2)}{E_s}\right]^{-1} \tag{2}$$

In Eq. (2), the parameters $E_i = 1141$ GPa and $\nu_i = 0.07$ represent the elastic modulus and Poisson ratio of the diamond indenter tip, respectively, and E_s and ν_s represent the elastic constants of the glass. Since the exact value of ν_s is unknown, we defined the modulus as $E = E_s / (1 - \nu_s^2)$.

The indentation depth responses show a marked indentation size effect (*ISE*) for the $Cu_{48}Zr_{48}Al_4$ alloy (Fig. 3), which reflects in a decrease of the modulus and hardness with increasing indenter displacement, h. With respect to the hardness, this effect is more pronounced for small indentation depths and diminishes as the displacement into surface increases, while no convergence towards a constant value is identified in the modulus depth profile up to the maximum indentation depth at around 2 μm. Although the *ISE* is usually found in crystalline materials [43], various reports have pointed-out similar effects also in metallic glasses [23,44–50]. The strain-induced softening due to the continuous creation and coalescence of excess free volume upon indentation was proposed as the origin for the *ISE* in amorphous alloys [44,47,49]. Plastic flow in metallic glasses is accompanied by dilatation, i.e., the creation of excess free volume [12,51]. Since the formation of additional free volume is proportional not only to the applied strain-rate, but also to the

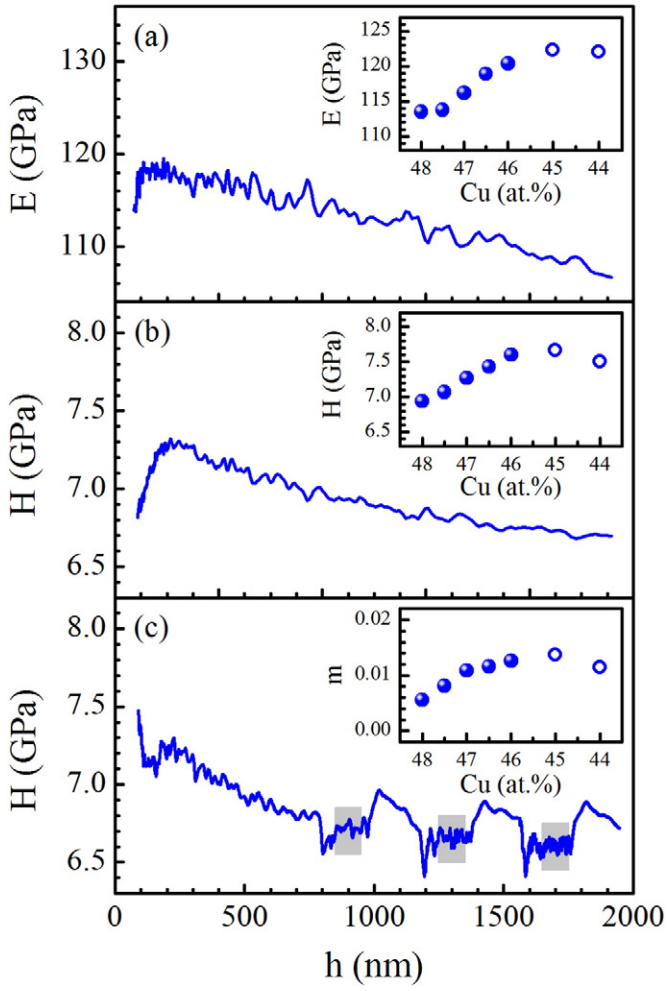

Fig. 3. Depth profiles of Young's modulus E and hardness H of the vitreous ternary $Cu_{48}Zr_{48}Al_4$ alloy, as determined by constant strain-rate indentations (a, b) and indentation with strain-rate jumps (c), respectively. The insets display the compositional dependence of the E, H and the strain-rate sensitivity m of ternary $(Cu_{0.5}Zr_{0.5})_{100-x}Al_x$ (x = 4, 5, 6, 7 and 8 at.%, filled symbols) and quaternary $Cu_{46-y}Zr_{46}Al_8Co_y$ (y = 1 and 2 at.%, open symbols) alloys on the Cu content. The values of E and H determined by the constant strain-rate indentations (a, b) were averaged between the upper 10% and lower 20% of each indentation depth profile. Their experimental errors are reflected by the size of the symbols. The grey shades in the strain-rate jump test (c) mark the intervals within which the different strain-rates were applied.

overall strain, metallic glasses tend to soften progressively in the course of an indentation experiment, leading to the observed *ISE* [44,49].

Besides the load dependence of the mechanical properties, a strong compositional effect is seen in the studied alloys. In the ternary $(Cu_{0.5}Zr_{0.5})_{100-x}Al_x$, the modulus increases linearly from 113.5 ± 0.8 GPa up to 120.4 ± 0.6 GPa as the Al content is raised from 4 to 8 at.% (inset in Fig. 3a), which is in good agreement with the observations of a previous nanoindentation study performed by Cheung and Shek [30], as well as other experimental techniques, such as ultrasonic echography [35,36] or uniaxial compression [33]. Likewise, the hardness increases from 6.94 ± 0.05 GPa up to 7.60 ± 0.04 GPa (inset in Fig. 3b). Both trends are in line with the compositional dependence of the glass-transition temperature described above, and confirm the apparent correlation between the thermal and mechanical properties of metallic glasses which has been demonstrated by Wang [52,53] for a variety of different alloys. These empirical relationships link the glass-transition temperature to mechanical characteristics, such as the modulus, hardness or strength [16,52]. Following this, it has been suggested that the mechanical properties of metallic glasses, in a similar manner as their glass-transition temperature, scale directly with the strength of the interatomic bonds [53,54]. However, in the present series of $(Cu_{0.5}Zr_{0.5})_{100-x}Al_x$ alloys, the glass-transition temperature, modulus or hardness increase monotonously with increasing Al content, although the mean atomic bonding energy as approximated from the weighted average of the atomization energies ΔH_{at} of each constituent, $U_0 = \sum_{i=1}^{n} f_i \Delta H_{at}^i$ [54], decreases when Cu (338 kJ/mol) and Zr (605 kJ/mol) are gradually replaced by Al (326 kJ/mol). This particular result supports a previous argument where the atomic structure of the Cu-Zr-Al alloys deviates substantially from the commonly considered structural model of a random arrangement of densely packed clusters of atoms [2,3]. In fact, adding Al to a binary $Cu_{50}Zr_{50}$ alloy induces distinct structural changes in the short- and medium-range order [55–57], e.g., by introducing new bonds with a more localized (covalent) character as compared to the metallic bonds. This was proposed to be one crucial factor for the increased thermal and mechanical stability of these alloys [55].

In contrast to the instantaneous elastic-plastic deformation, the time-dependent indentation response of the ternary Cu-Zr-Al and quaternary Cu-Zr-Al-Co alloys was evaluated by means of a nanoindentation strain-rate jump test, as exemplarily shown for the $Cu_{48}Zr_{48}Al_4$ alloy in Fig. 3c. All alloys tested in this study exhibit a weak but positive rate-dependence of the hardness. This comes as a surprise at first glance, since the hardness of metallic glasses is usually referred-to as rate-independent [15]. Nevertheless, this topic still remains a subject of controversy, as positively depending [15,27,48,50,58–63], negatively depending [64,65] and rate-independent hardness values [66–73] have been reported for metallic glasses over the past years. In order to quantify the rate-dependence of the hardness in the current series of ternary Cu-Zr-Al and quaternary Cu-Zr-Al-Co alloys and to reveal the relative impact of the Al or Co content, the strain-rate sensitivity was deduced from a linear regression between the logarithm of the hardness, $\ln(H)$, and the logarithm of indentation strain-rate, $\ln(\dot{\varepsilon}_i)$ [37]:

$$m = \frac{\partial \ln(H)}{\partial \ln(\dot{\varepsilon}_i)}, \tag{3}$$

where $\dot{\varepsilon}_i$ is equal to one half of the applied strain-rate, $\dot{\varepsilon}$, for materials with depth-independent hardness [74]. In light of the *ISE* mentioned above, the question arises as to whether the hardness decrease in the nanoindentation strain-rate jump tests originates from the gradually reduced strain-rate, or from the continuously increasing load. For that reason, the same method was also applied to the well-studied $Zr_{52.5}Cu_{17.9}Ni_{14.6}Al_{10}Ti_5$ alloy, commonly known as Vitreloy 105 (Vit105) [75], and the results were compared with previous findings of a constant strain-rate nanoindentation experiment, conducted by Cheng et al. [48]. Using the nanoindentation strain-rate jump test, a strain-rate sensitivity of 0.0086 was obtained here, which corresponds very well to the value of $m = 0.0076$ derived from constant strain-rate indentations [48]. This result demonstrates that the *ISE* has only a minor influence on the strain-rate sensitivities determined by the method used in this report, due to an appropriate combination of a large initial displacement prior to the consecutive strain-rate jumps and the low applied strain-rates [50]. The compositional dependence of the strain-rate sensitivity is shown as a function of the Cu content in the inset in Fig. 3c. For metallic glasses, a decrease in m signifies a transition from homogeneous towards non-homogeneous flow with strong localization of plastic deformation in individual, narrow shear bands [51]. For the ternary $(Cu_{0.5}Zr_{0.5})_{100-x}Al_x$ alloys, the strain-rate sensitivity increase monotonically with increasing Al content, from 0.0056 ($Cu_{48}Zr_{48}Al_4$) up to 0.0126 ($Cu_{46}Zr_{46}Al_8$). The magnitude of these values indicates an almost ideal plastic flow [15,27], which corresponds to the low rate-dependence of the hardness seen in the strain-rate jump test of the $Cu_{48}Zr_{48}Al_4$ alloy (Fig. 3c). Apart from this, the increasing strain-rate sensitivity implies a change in the indentation response of these alloys through a homogenization of plastic flow [76–78].

Regarding the quaternary $Cu_{46-y}Zr_{46}Al_8Co_y$ alloys, the present study clearly illustrates the importance of the type and concentration of the alloying species. After the addition of 1 at.% Co at the expense of Cu, the modulus ($Cu_{46}Zr_{46}Al_8$: $E = 120.4 \pm 0.6$ GPa and $Cu_{45}Zr_{46}Al_8Co_1$: $E = 122.4 \pm 0.5$ GPa), hardness ($Cu_{46}Zr_{46}Al_8$: $H = 7.60 \pm 0.04$ GPa and $Cu_{45}Zr_{46}Al_8Co_1$: $E = 7.67 \pm 0.05$ GPa) and strain-rate sensitivity ($Cu_{46}Zr_{46}Al_8$: $m = 0.0126$ and $Cu_{45}Zr_{46}Al_8Co_1$: $m = 0.0138$) increase somewhat, but to a lower extent as compared to the addition of Al. Upon further increasing the Co concentration, modulus ($Cu_{44}Zr_{46}Al_8Co_2$: $E = 122.1 \pm 0.5$ GPa), hardness ($Cu_{44}Zr_{46}Al_8Co_2$: $H = 7.51 \pm 0.05$ GPa) and strain-rate sensitivity ($Cu_{44}Zr_{46}Al_8Co_2$: $m = 0.0115$) start to decrease. Similar observations have been made also by Chen et al. [79] and Pan et al. [80,81] in ternary Cu-Zr-Al alloys containing up to 2 at.% of Ti, Fe and Ta, respectively, or more recently by Zhou et al. [82] in a report concerning the effect of Sn on the microstructure, thermal stability and mechanical properties of such alloys. In the latter studies, both the plasticity and fracture strength were found to increase with minor additions of Fe or Sn. This observation was related to nanoscale precipitation of a mechanically more resistant Zr-rich glassy phase within a softer Cu- and Al-rich glass matrix, which promotes the multiplication, branching and deflection of shear bands [80–82]. However, for Sn contents exceeding a threshold value, the beneficial effects were counterbalanced by the precipitation of crystals [82]. The present results indicate that similar effects control the mechanical performance also of the quaternary Co-containing alloys.

3.3. Serrated flow

Plastic deformation in metallic glasses at high stresses and low temperatures is inhomogeneous with a strong concentration of the strain in a few narrow shear bands [51]. Under bending or tensile loading conditions, these shear bands nucleate and propagate along a single plane in the direction of the maximum shear stress throughout the material [4]. As opposed to this, the plastic flow in an indentation experiment is restricted to a very small volume adjacent to the indenter tip. Consequently, the propagation of a shear band arrests as soon as the strain imposed on the sample surface is accommodated by a cooperative shear motion of the atoms inside the band, whereas continuous deformation is achieved via successive operation of individual shear bands [8].

The formation and propagation of shear bands in metallic glasses upon indentation gives rise to sudden displacement bursts, which manifest in the form of small serrations or “pop-ins” in the load-displacement curve [68]. In Fig. 4, the loading portions of representative indentations on ternary $(Cu_{0.5}Zr_{0.5})_{100-x}Al_x$ alloys containing 4, 6 and 8 at.% Al, respectively, are presented. For clarity, the curves recorded at loading rates, dP/dt, of 0.1, 1 and 10 mN/s, are shifted horizontally. Obviously, magnitude and appearance of the displacement bursts not only depend on composition, but also on the loading conditions [67,84–86]. At the lowest loading rate of 0.1 mN/s, the loading curve of the $Cu_{48}Zr_{48}Al_4$ alloy (Fig. 4a) exhibits pronounced serrations, which are accompanied by an abrupt increase of the displacement at almost constant load. As the loading rate increases from 0.1 to 10 mN/s, number and size of the serrations decrease. Their appearance in the load-displacement curve transforms into small fluctuations or waves as compared to the discrete steps seen at lower loading rate. This indicates a rate-dependent inhomogeneous-to-homogeneous transition in local flow, an effect which has previously been assigned to kinetic limitations during shear band formation: at lower loading rate, a single shear band may rapidly accommodate the strain and relax the residual stresses through a discrete displacement burst, while at higher loading rates a single shear band may not operate fast enough to accommodate the imposed strain and, as a result, multiple shear bands are activated simultaneously [67,87].

In addition to the loading rate effect, the ternary Cu-Zr-Al alloys also display a marked compositional dependence of their flow behavior. At the lowest loading rate of 0.1 mN/s the loading curve of $Cu_{48}Zr_{48}Al_4$ (Fig. 4a) appears to be serrated more strongly than for the $Cu_{47}Zr_{47}Al_6$ (Fig. 4b) and $Cu_{46}Zr_{46}Al_8$ alloys (Fig. 4c). Interestingly, these differences are more pronounced at smaller loading rates, but level-off for more rapid indentation. To better illustrate this finding, the contribution of serrated flow on the total plastic deformation was estimated, following the procedure introduced by Schuh et al. [67,84,87,88]. The indentation load-displacement curves were first separated into three portions, an elastic deformation, $h_{elastic}$, a discrete plastic deformation, $h_{discrete}$, and a continuous plastic deformation, $h_{continuous}$. Since the elastic deformation recovers during unloading, the relative contribution of discrete plasticity on the total plastic deformation, or the discrete plasticity ratio, $h_{discrete}/h_{plastic}$, is determined from the sum of each individual pop-in, $h_{discrete} = \Sigma h_{pop\text{-}in}$, divided by the residual indentation depth after releasing the load. The results of this analysis are visualized in Fig. 5 for the ternary $(Cu_{0.5}Zr_{0.5})_{100-x}Al_x$ alloys containing 4, 6 and 8 at.% Al, respectively. Each data point represents the mean value of $h_{discrete}/h_{plastic}$ from up to 20 independent indentations. Referring again to the $Cu_{48}Zr_{48}Al_4$ alloy, the discrete plasticity ratio continuously increases with a decrease in loading rate over a range of three decades. Similar observations are made on both $Cu_{47}Zr_{47}Al_6$ and $Cu_{46}Zr_{46}Al_8$. However, in comparison to the $Cu_{48}Zr_{48}Al_4$ alloy, the increase of the discrete plasticity ratio proceeds more slowly for higher Al contents, which leads to a growing divergence between the relative contribution of serrated flow on the indentation response of the three different alloys as the loading rate decreases. Large ratios of $h_{discrete}/h_{plastic}$ are usually related to alloys in which plastic flow is driven by the activation of a small number of large shear bands, while lower values of $h_{discrete}/h_{plastic}$ are related to the operation of multiple, but very narrow shear bands [85,86]. Hence, the compositional dependence of the discrete plasticity ratio for the present $(Cu_{0.5}Zr_{0.5})_{100-x}Al_x$ alloys reflects stronger localization of plastic flow in the alloys which contain relatively smaller amounts of Al. This finding verifies the previous interpretation of the strain-rate jump tests, where an increasing strain-rate sensitivity with increasing Al content was detected. Moreover, these results unambiguously demonstrate the applicability of the strain-rate sensitivity as an indicator for the flow behavior of metallic glasses upon indentation.

3.4. Initiation of heterogeneous plastic flow

The serrated flow behavior not only depends on the composition of the metallic glass or the applied loading rate, but also on the geometry of the indenter tip. The highest values of $h_{discrete}/h_{plastic}$ are commonly achieved for sharp, geometrically self-similar indenter tips, such as cube corners [89]. However, the use of a spherical indenter enables detailed analysis of the elastic deformation regime, since the transition towards an elastic-plastic deformation is shifted to higher loads and displacements as the tip radius increases [90]. Fig. 6 displays the loading portion of a typical load-displacement curve of the $Cu_{48}Zr_{48}Al_4$ alloy from a constant loading-rate indentation experiment using a conical indenter. Prior to the first pop-in, the loading curve exhibits a smooth and parabolic shape, which can be described by Hertz's law for an elastic contact [91]:

$$P = \frac{4}{3} E_r \sqrt{R h^3}, \tag{4}$$

with $E_r = 108.0$ GPa. In the later stages, the indentation response of the $Cu_{48}Zr_{48}Al_4$ alloy deviates substantially from the ideal elastic behavior, indicating that the transition to plastic deformation, i.e., the onset of yielding, occurs exactly at the point where the first pop-in appears in the loading curve. Thus, the maximum shear stress, τ_m, at the initiation of the first pop-in can be regarded as the shear strength parameter of the alloy [90]. In spherical indentation, τ_m reaches its

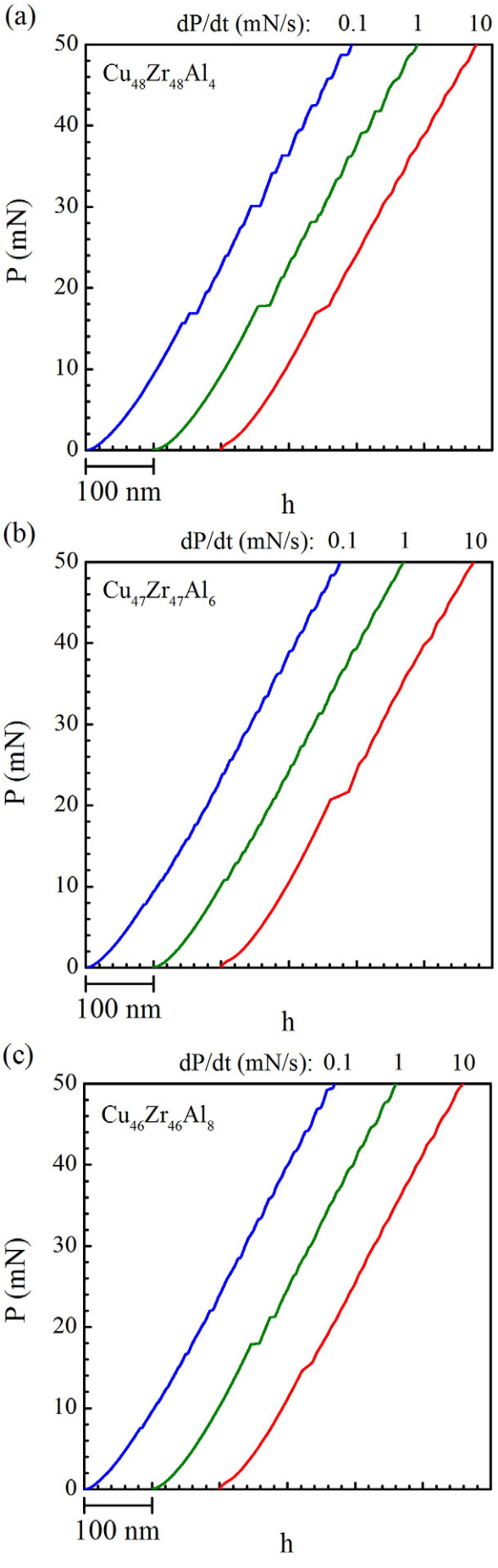

Fig. 4. Loading portions of representative load-displacement, *P-h*, curves of vitreous ternary $Cu_{48}Zr_{48}Al_4$ (a), $Cu_{47}Zr_{47}Al_6$ (b) and $Cu_{46}Zr_{46}Al_8$ (c) alloys. Indents with a maximum load of 50 mN were created at constant loading rates, *dP/dt*, of 0.1, 1 and 10 mN/s, respectively, using a conical indenter with an effective tip radius of 4.53 μm. For clarity, the curves recorded at different loading rates are shifted horizontally.

maximum at a distance of about half the contact radius below the sample surface [91],

$$\tau_m = 0.295p_0 = 0.443p_m = 0.443\left(\frac{16PE_r^{\,2}}{9\pi^3R^2}\right), \tag{5}$$

where p_0 and p_m are the maximum and mean contact pressures, respectively. The constant of 0.295 was calculated using an average value of $\nu = 0.365$ [32,35] for all alloys tested. It is important to note that for a given metallic glass, the onset of yielding does not always occur at the same load. In fact, there exists a distribution of strengths necessary for the initiation of plastic flow, as already reported in earlier studies [14,23]. For example, loads ranging from 7.84 up to 22.2 mN were required to observe the first pop-in, $P_{pop\text{-}in}$, in the $Cu_{48}Zr_{48}Al_4$ alloy (inset in Fig. 6), although all indentations were performed under the same experimental conditions. In very recent reports, this phenomenon has at least partly been attributed to the spatial heterogeneity in the local atomic configurations inherent to metallic glasses [19,23–26,92,93]. The wide scatter of strength values can more readily be understood in terms of the thermally activated and stress-biased model for yielding [94]. Yielding can occur at any stress when the thermal energy is high enough, whereby the probability for yielding increases exponentially with increasing load. This also reflects in the cumulative distribution of τ_m of the ternary $(Cu_{0.5}Zr_{0.5})_{100-x}Al_x$ and quaternary $Cu_{46-y}Zr_{46}Al_8Co_y$ alloys (Fig. 7a). Interestingly, the slope of these curves seems to be practically unaffected by the Al or Co content, except for the small discontinuity in the cumulative distribution of the $Cu_{44}Zr_{46}Al_8Co_2$ alloy. Apart from that, with increasing Al content the entire curve and also the upper limit of τ_m is continuously shifted to higher values ($Cu_{48}Zr_{48}Al_4$: $\tau_m = 3.86$ GPa and $Cu_{46}Zr_{46}Al_8$: $\tau_m = 4.10$ GPa). With the introduction of minor amounts of Co ($Cu_{46}Zr_{46}Al_8Co_1$: $\tau_m = 4.24$ GPa) a similar effect is initially achieved, whereas at higher Co contents the upper limit of τ_m starts to decrease slightly ($Cu_{46}Zr_{46}Al_8Co_1$: $\tau_m = 4.17$ GPa). As a result, τ_m follows the earlier described compositional trends of *E* or *H*, supporting again the widely accepted theory of a direct link between the elastic properties, plastic deformation and strength in metallic glasses [16,52].

In the thermally activated and stress-biased model for yielding, the activation volume of the nucleation event at the onset of yielding can be estimated by means of a statistical analysis of the distribution of strengths at the first pop-in [94]. This model has successfully been applied by Choi et al. [14] to metallic glasses. Thereby, the cumulative distribution of strengths (presented in Fig. 7a) is described as a function of the instantaneous shear stress, τ, beneath the indenter [94],

$$f = 1 - exp\left[-\frac{kT\dot{\gamma}_0}{V^*\left(\frac{d\tau}{dt}\right)}\, exp\left(-\frac{\Delta F^*}{kT}\right)\, exp\left(-\frac{\tau V^*}{kT}\right)\right], \tag{6}$$

where kT is the thermal energy, k is Boltzmann constant, and T the temperature. The parameter $\dot{\gamma}_0$ is the attempt frequency and ΔF^* denotes the Helmholtz activation energy, i.e. the intrinsic nucleation barrier in the absence of external stimuli. For indentations performed at constant loading rates, the stress rate, $d\tau/dt$, is also constant. Eq. (6) can be rewritten as

$$\ln\left[\ln\left(1-f\right)^{-1}\right] = \left\{\frac{\Delta F^*}{kT} + \ln\left[\frac{kT}{V^*(d\tau/dt)}\right]\right\} + \left(\frac{V^*}{kT}\right)\tau \tag{7}$$

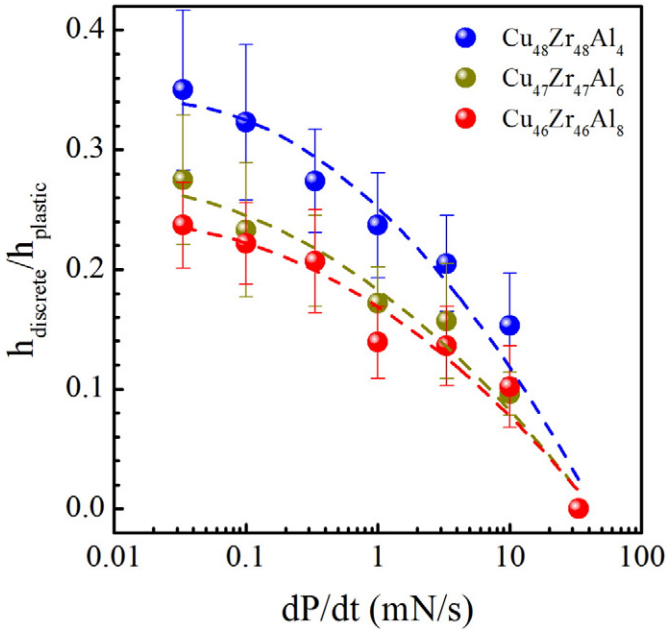

Fig. 5. Loading rate dependence, dP/dt, of the relative contribution of discrete plastic flow, $h_{discrete}$, on the total plastic deformation, $h_{plastic}$, for ternary $(Cu_{0.5}Zr_{0.5})_{100-x}Al_x$ metallic glasses containing 4 at.% Al (blue circles), 6 at.% Al (yellow circles) and 8 at.% Al (red circles), respectively. The dashed lines are guides for the eyes.

By substituting τ with τ_m, the activation volume V^* can be derived from the slope of the linear regression curve. Plots of $\ln[\ln(1-f)^{-1}]$ as a function of τ_m are displayed in Fig. 7b. For the determination of V^* the upper and lower 10% of each profile were excluded. In every case, a correlation factor, R^2, higher than 0.95 was obtained, except for the $Cu_{44}Zr_{46}Al_8Co_2$ alloy ($R^2 = 0.86$).

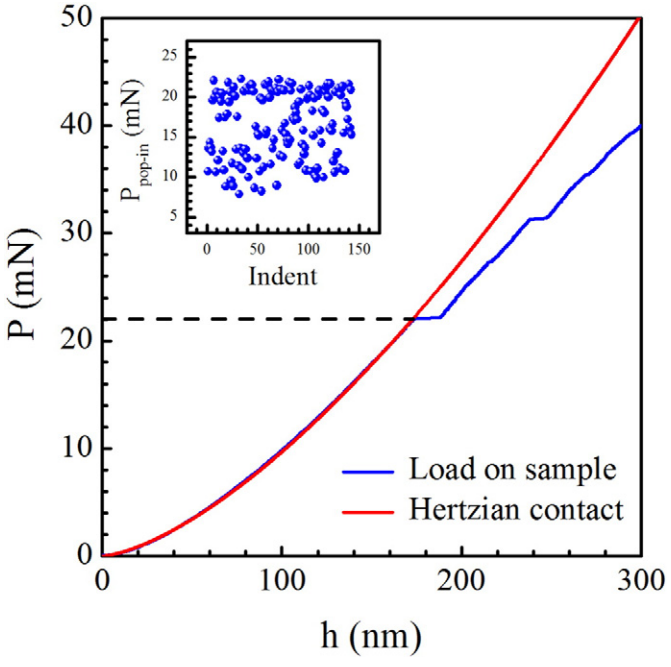

Fig. 6. Loading portion of a representative load-displacement, *P-h*, curve of a vitreous ternary $Cu_{48}Zr_{48}Al_4$ alloy (blue curve). The indent with a maximum load of 50 mN was performed at a constant loading rate of 1 mN/s, using a conical indenter. The red curve displays the ideal elastic response according to Hertz. Dashed line marks the load, $P_{pop\text{-}in}$, at which the first displacement burst appears. In the inset, the distribution of $P_{pop\text{-}in}$ obtained from >140 independent indentations is illustrated.

According to the original concept of Argon [12], yielding in metallic glasses is governed by a cooperative rearrangement of a group of atoms (STZ) [13]. Using the activation volumes determined above, the size of this most fundamental carrier for plastic flow in metallic glasses can be estimated following the cooperative shear model of Johnson and Samwer [16]. As already noted, a STZ is defined by its transience, i.e., its operation is induced through externally applied stresses [8]. For the activation of a STZ, these stresses have to overcome a potential energy barrier, W, which can be expressed by the following equation [16]:

$$W = 4CG_0\gamma_C{}^2\left(1-\frac{\tau_{CT}}{\tau_{C0}}\right)^{3/2}\xi\Omega, \tag{8}$$

where G_0 is the shear modulus at $T = 0$ K, τ_{CT} and τ_{C0} are the shear strengths at finite temperature and $T = 0$ K, respectively, and Ω stands for the volume of a STZ. The parameters ξ and C are constants that are equal to 3 and approximately 1/4, respectively. Differentiating and rearranging Eq. (8) yields [14]:

$$\Omega = \frac{\tau_{C0}}{6CG_0\gamma_C{}^2\xi\left(1-\frac{\tau_{CT}}{\tau_{C0}}\right)^{1/2}}V^* \tag{9}$$

For the shear strain at yielding, $\gamma_C = \tau_{CT}/G_T$, Johnson and Samwer [16] introduced a scaling law, which is based on experimental data of 30 different alloys:

$$\gamma_C = \frac{\tau_{CT}}{G_T} = 0.036-0.016\left(\frac{T}{T_g}\right)^{0.62} \tag{10}$$

The shear modulus in a metallic glass exhibits only a weak temperature-dependence and does not affect the calculated STZ volume [14]. As a consequence, for a given glass-transition temperature, the STZ volume of a metallic glass can be derived directly from its activation volume by means of Eqs. (9) and (10). Once the STZ volume is determined, the number of atoms involved in the collective reorganization are approximated assuming a random arrangement of densely packed hard spheres with the average atomic radius $r = (\sum_{i=1}^{n} f_i r_i)^{1/3}$, where f_i and r_i are the atomic fraction and radius of each element, respectively [15]. The results of these calculations are summarized in Table 2.

For the ternary Cu-Zr-Al alloys, the STZ volume remains almost constant within a narrow interval of 0.277 to 0.306 nm^3, which corresponds to clusters of about 22–24 atoms per STZ. Equivalent results are obtained for the quaternary Cu-Zr-Al-Co alloys, but with a slightly broader distribution of the STZ volume and size, that is, 0.255 nm^3 (20 atoms) and 0.332 nm^3 (26 atoms) for the $Cu_{45}Zr_{46}Al_8Co_1$ and $Cu_{44}Zr_{46}Al_8Co_2$ alloy, respectively. These values are in fairly good agreement with previous experimental studies on comparable alloys of the Cu-Zr-Al ternary system [21,28]. Furthermore, the insensitivity of the STZ volume to small compositional variations in both the ternary Cu-Zr-Al and quaternary Cu-Zr-Al-Co alloys indicates a negligible influence of alloying components. The present findings are in contrast to a very recent report of Ma et al. [28], who have found a tremendous increase of the STZ volume by about 60% after the addition of minor amounts of Ti to a ternary Cu-Zr-Al alloy. The authors of this study have attributed their results to the creation of excess free volume, which facilitates the formation of larger STZs, although in earlier studies, the opposite effect of the free volume content on the STZ volume has been observed for metallic glasses subjected to thermal treatment [18,23,26]. Annealing of metallic glasses leads to structural relaxation, which is often accompanied by local rearrangements in the atomic configuration and an associated redistribution and reduction of the free volume due to densification [8]. A major consequence of structural relaxation is a progressive reduction of the

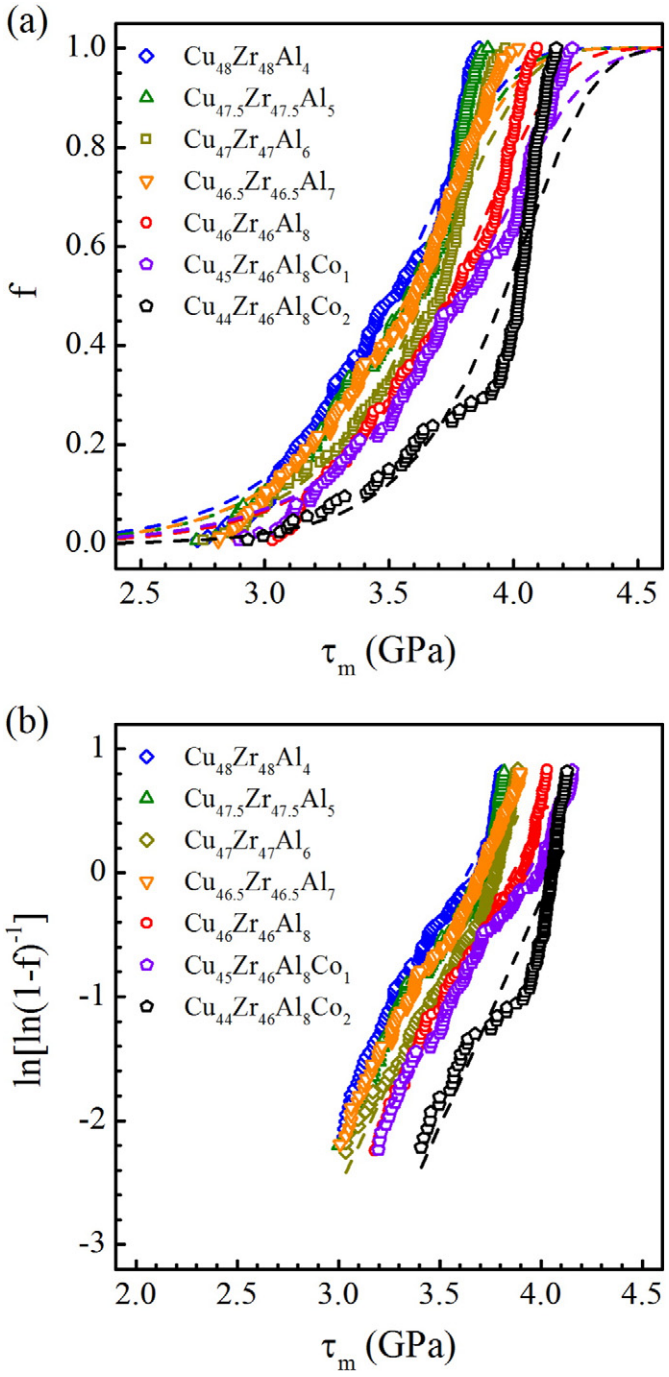

Fig. 7. Statistical analysis of the first pop-in for the ternary $(Cu_{0.5}Zr_{0.5})_{100-x}Al_x$ (x = 4, 5, 6, 7 and 8 at.%) and quaternary $Cu_{46-y}Zr_{46}Al_8Co_y$ (y = 1 and 2 at.%) alloys studied, showing the cumulative distribution of the maximum shear stress, τ_m, associated with the first pop-in (a) and $\ln[\ln(1-f)^{-1}]$ as a function of τ_m (b). Dashed lines are fits to the experimental data using Eqs. (6) and (7), respectively.

degree of structural disorder or heterogeneity [23]. However, local "defects" in the glass structure, such as a larger free volume or an increased structural heterogeneity, are assumed to act as preferential sites for shear transformations [4]. As a result, several researchers have tried to utilize the width of the strength distribution as a mechanical probe for the spatial heterogeneity in the local atomic configuration of metallic glasses, i.e., the narrower the distribution of strengths, the lower the number of available sites for shear transformation and, hence, the more homogeneous the structure of the alloy [23,24,26]. Since the activation volume of a STZ is directly linked to the distribution of strengths (Eq. (7)), smaller STZs are expected to emerge in glasses with pronounced structural heterogeneity, and vice versa. With respect to the current series of ternary Cu-Zr-Al and quaternary Cu-Zr-Al-Co alloys, the marginal differences in the STZ volumes imply that Al and Co do not alter significantly structural heterogeneity of the glass. The marked differences in the STZ volumes seen in previous reports might be the consequence of drastic structural changes, as induced by either strong compositional variations, e.g., via exchanging the main atomic species and bonding characteristics [17,19,21,24], or local rearrangements in the atomic configuration upon thermal treatment [18,23,24,26,95]. Nonetheless, during spherical indentation experiments on the $(Cu_{0.5}Zr_{0.5})_{100-x}Al_x$ alloys a considerable change in the shear band formation, with a decreasing tendency for shear localization, is observed when the Al content is increased (Fig. 4).

A commonly accepted theory for the relationship between the STZ volume and the shear band formation has not yet been established and its influence on the fracture behavior of metallic glasses is still far from being understood [8]. Choi et al. [23] or, more recently, Cao et al. [18] and Li et al. [26], have investigated the STZ formation in metallic glasses with regard to the degree of structural relaxation. In these studies, a marked increase in the STZ volume was detected after thermal treatment. Since structural relaxation in metallic glasses involves a transition towards a more densely packed atomic configuration, Choi et al. [23] have argued that shear transformations in structurally relaxed glasses (as compared to as-cast alloys) involve a higher number of collectively rearranging atoms. Clearly, higher packing efficiency commonly restricts the local movement of atoms, which reduces the shear-banding ability. Accompanied by this, the toughness of metallic glasses reduced [8,24]. Jiang et al. [95] have reported on the effect of structural relaxation on STZ formation and observed a tough-to-brittle transition in the fracture behavior upon annealing, but in contrast to the studies mentioned before, the STZ volume was found to decrease after thermal treatment. Jiang et al. [95] explained this finding as follows: The presence of larger STZs in tough metallic glasses induces large stress gradients in some region of the material, which facilitates the generation of excess free volume and promotes plastic flow through the formation and interaction of multiple shear bands. In more brittle metallic glasses, cracks can easily propagate throughout the material since a large amount of smaller STZs needs to be activated to form a shear band. As a consequence, plastic flow becomes more difficult.

3.5. Shear transformation zones and plasticity of metallic glasses

Extensive shear banding and high fracture toughness are normally preferred in metallic glasses with low shear modulus (low resistance against plastic flow) and high bulk modulus (strong resistance against volume dilatation controlled crack propagation), or, in others words

Table 2
Shear transformation zones (STZ) in the vitreous ternary $(Cu_{0.5}Zr_{0.5})_{100-x}Al_x$ (x = 4, 5, 6, 7 and 8 at.%) and quaternary $Cu_{46-y}Zr_{46}Al_8Co_y$ (y = 1 and 2 at.%) alloys. Following the cooperative shear model of Johnson and Samwer [16], the STZ volume, Ω, and the number of atoms, N, involved in the shear transformations were estimated from the activation volume of a STZ, V^*, using a statistical analysis of the maximum shear stress at the onset of yielding. Ω_{flow} and N_{flow} depict the volume and size of the plastic flow events, respectively, as determined by means of the strain-rate sensitivity according to Pan et al. [15] The Poisson ratio, ν, was taken from Ref. [35].

Composition (at.%)	ν	Statistical analysis			Strain-rate sensitivity	
		V^* (nm^3)	Ω (nm^3)	N	Ω_{flow} (nm^3)	N_{flow}
$Cu_{48}Zr_{48}Al_4$	0.370	0.0127	0.277	22	12.15	952
$Cu_{47.5}Zr_{47.5}Al_5$	0.372	0.0131	0.286	23	8.27	650
$Cu_{47}Zr_{47}Al_6$	0.367	0.0140	0.306	24	5.99	473
$Cu_{46.5}Zr_{46.5}Al_7$	–	0.0128	0.281	22	5.52	437
$Cu_{46}Zr_{46}Al_8$	0.366	0.0129	0.284	23	4.82	384
$Cu_{45}Zr_{46}Al_8Co_1$	–	0.0116	0.255	20	4.50	358
$Cu_{44}Zr_{46}Al_8Co_2$	–	0.0151	0.332	26	5.51	438

high Poisson ratio [96]. Although this simple one-to-one relationship and the existence of a critical Poisson ratio for the tough-to-brittle transition remains doubtful, the Poisson ratio is nowadays widely applied as an indicator for plasticity, for example, when fundamental deformation processes in metallic glasses are related to their fracture behavior [4]. Liu et al. [97] have employed a dynamic mechanical analysis to characterize the compositional dependence of the activation energy and volume of STZs formed in different metallic glasses. Their analysis has revealed a rough trend showing the operation of smaller STZs in alloys with higher Poisson ratio on the one hand, and the occurrence of larger STZs in more brittle alloys with lower Poisson ratios on the other hand. Liu et al. [97] concluded that smaller STZs, rather than larger ones as suggested by Jiang et al. [95], are responsible for the nucleation of multiple shear bands and the enhanced plasticity in metallic glasses. A similar trend was noticed by Ma et al. [21], who have determined the STZ volume of metallic glassy films through a statistical survey of the maximum shear stress at the onset of yielding, as described above, while the opposite behavior (a decrease of the STZ volume with increasing Poisson ratio) was observed by Pan et al. [15]. In the latter study, nanoindentation experiments with strain-rate jumps were conducted and the STZ volume was derived from the strain-rate sensitivity by means of the following equation:

$$\Omega = \frac{kT}{C' m H}, \tag{11}$$

where $C' = \frac{2R\xi}{\sqrt{3}} \frac{G_0 \gamma_C{}^2}{\tau_{c0}} \left(1 - \frac{\tau_{CI}}{\tau_{c0}}\right)^{1/2}$ is a constant that originates from the cooperative shear model of Johnson and Samwer [16]. With this method, Pan et al. [15] obtain relatively large STZ volumes of about 2 to 7 nm^3, which correspond to clusters of approximately 200 to 700 atoms. For comparison, shear transformations at the onset of yielding are confined to a local volume of just a few tens of atoms [17,21]. However, since the hardness describes the resistance against plastic flow rather than its initiation [98], the volume determined by the strain-rate sensitivity is assumed to depict a plastic flow unit involving a number of cooperative shear transformations with a total volume of a few hundred atoms [4]. Regarding the alloys examined in the current report, we first want to recall the monotonic increase of the strain-rate sensitivity with increasing Al content in the ternary $(Cu_{0.5}Zr_{0.5})_{100-x}Al_x$ alloys and the accompanied gradual homogenization of plastic flow. As the hardness increases in a similar manner, the calculated volume of the local flow units that govern plastic deformation during the nanoindentation experiment continuously decreases from 12.14 nm^3 (~950 atoms) at 4 at.% Al down to 4.82 nm^3 (~380 atoms) at 8 at.% Al. These values as well as the results for the quaternary Cu-Zr-Al-Co alloys are summarized in Table 2. To avoid confusions with the STZ volume determined at the onset of yielding, the volume of the flow units derived from the strain-rate sensitivity is denoted by Ω_{flow}. Interestingly, while the STZ volume is nearly independent of small compositional changes, the size of the flow units varies substantially. Since the latter parameter reflects a collection of simultaneously operating STZs [4], a larger quantity of STZs are activated in the alloys with lower Al concentrations as compared to the alloys containing higher amounts of Al. These STZs are strongly localized and can easily percolate into a shear band. Opposite to this, the reduced quantity of STZs at higher Al contents combined with their broader distribution impedes the formation of shear bands. Consequently, crack propagation is favored over plastic flow [95]. These results also coincide with the compositional dependence of plasticity in the $(Cu_{0.5}Zr_{0.5})_{100-x}Al_x$ ternary system. The addition of Al into a binary $Cu_{50}Zr_{50}$ alloy initially improves the plasticity of the resulting metallic glass, but this effect is limited to small concentrations of up to 5 at.% Al. Afterwards, with further incorporation of Al, the plasticity drops rapidly [33–35]. Along with this change in plasticity, also the Poisson ratio increases at first and exhibits a maximum at around 5 at.% Al [32,35].

It now appears reasonable to validate whether this theory can also be transferred to other metallic glasses. For this purpose, the strain-rate sensitivity of the ternary Cu-Zr-Al alloys is plotted against the Poisson ratio in Fig. 8, together with literature values from impression creep experiments [18,27,99,100], nanoindentation strain-rate jump tests [15,22,62] as well as indentations performed at constant strain-rates [48]. As supplementary information, the size of the symbols represents the number of atoms, N_{flow}, which undergo a collective reorganization during the activation of a plastic flow event. We have initially to point out that the evaluation and comparison of the strain-rate sensitivity of different alloy systems or varying experimental setups is not straightforward. Previous studies revealed, for example, a distinct size- and rate-dependence in the indentation creep behavior of metallic glasses. That is, for indentations created at higher loading rates, larger creep displacements and by extension higher strain-rate sensitivities were obtained during the subsequent holding period [76,77,101]. However, this rate dependence seems to occur only at low loads or displacements and levels-off as the penetration depth increases [101]. Another crucial aspect in this regard is the proper definition of the steady-state creep regime, but also the structural heterogeneity of metallic glasses has to be considered [102]. Furthermore, it should to be noted that metallic glasses usually exhibit a zero or slightly negative strain-rate sensitivity under quasi-static or dynamic loading conditions [65]. On the contrary, positive values were determined in nanoindentation strain-rate jump tests both in the present and previous reports [15,22,62]. Bhattacharyya et al. [65] suggested that the positive rate-dependence of hardness observed in several nanoindentation studies might be an experimental artifact that arises from the piling-up of material around the indenter tip due to plastic flow. This phenomenon becomes more pronounced as the loading rate increases, resulting in a growing discrepancy between the hardness values and strain-rate sensitivity derived from the topography of the residual indents, and the values which were calculated via Oliver and Pharr's method [38]. Nevertheless, the results illustrated in Fig. 8 reveal a very interesting trend. In general, low strain-rate sensitivities and large-sized flow units are found for compositions with higher Poisson ratio and higher plasticity, e.g., Pd-, Pt-, Zr- or Cu-based alloys. On the other side, larger strain-rate sensitivities and stronger variations in the size of the plastic flow units are possible for very low Poisson ratio, covering the region of the extremely brittle Mg-based alloys, but also metallic glasses with low glass-transition temperatures such as Ce- or La-based materials [103]. Pan et al. [22] have detected an increased strain-rate sensitivity and reduced size of the plastic flow units in a $Zr_{70}Ni_{16}Cu_6Al_8$ alloy after undergoing structural relaxation. Combining both results with our present findings, we can conclude that the plasticity of metallic glasses is closely related to their tendency towards the localized initiation of multiple STZs and the ability of these STZs to accumulate into large-sized plastic flow units. Moreover, our observations confirm an earlier hypothesis that the presence of larger flow units generates higher internal gradients of the applied stress, which promotes the generation of excess free volume and improves the plasticity of a metallic glass through the multiplication and branching of shear bands [15,95].

Although the above analysis provides further insight into the relationships between shear transformations, shear banding and plasticity in metallic glasses, an explanation for the reduced capability of STZ formation in ternary $(Cu_{0.5}Zr_{0.5})_{100-x}Al_x$ alloys with increasing amounts of Al is still missing. It has already been stated that shear transformations in metallic glasses are activated through an externally applied shear stress. In unstressed metallic glasses this cooperative rearrangement is hindered by a potential energy barrier, which is defined as [16]:

$$W = \frac{8}{\pi^2} G \gamma_C{}^2 \xi \Omega \tag{12}$$

However, the activation volume of shear transformation and the activation energy barrier for the operation of a STZ can vary significantly

among different metallic glasses [17,19,21]. For that reason, Liu et al. [103] proposed to normalize the activation energy barrier to the STZ volume and focus on the analysis of the barrier energy density, ρ, which needs to be overcome for STZ activation:

$$\rho = \frac{W}{\Omega} = \frac{8}{\pi^2} G\gamma_C{}^2\xi \tag{13}$$

Since $\gamma_C = 0.0267$ and $\xi = 3$ are constants within the cooperative shear model of Johnson and Samwer [16], the energy barrier density depends exclusively on the shear modulus, $G = E/(2-2\nu)$. As a reminder, the elastic modulus in the $(Cu_{0.5}Zr_{0.5})_{100-x}Al_x$ ternary system increases almost linearly with Al concentration, while at the same time the Poisson ratio decreases slightly for compositions with >5 at.% of Al [32,35]. As a consequence, also the shear modulus progressively increases. This effect is accompanied by a rise in the barrier energy density for the activation of a STZ and the enhanced resistance against the nucleation of shear transformation in the ternary $(Cu_{0.5}Zr_{0.5})_{100-x}Al_x$ alloys containing larger amounts of Al.

4. Conclusions

In summary, the addition of Al significantly improves the thermal stability of binary $Cu_{50}Zr_{50}$ alloys, but also tremendously changes the mechanical performance of the metallic glasses. This reflects in a continuous increase of the modulus, hardness and strain-rate sensitivity, whereby the latter indicates a reduced tendency for shear localization upon Al alloying. Accompanied by this, a gradual change in the indentation response with an apparent inhomogeneous-to-homogeneous transition in plastic flow has been observed. Using a statistical analysis of the maximum shear stress associated with the initiation of the first pop-in in the load-displacement curves of spherical indentations, the activation volume for plastic flow at the onset of yielding was determined. Following the cooperative shear model of Johnson and Samwer [16], the activation volume was employed for an experimental accession on the compositional dependence of the activation barrier, size and distribution of the shear transformations zones (STZs) of ternary Cu-Zr-Al alloys. It has been demonstrated that the STZ size does not change significantly upon Al alloying and encompasses a local volume of around 22–24 atoms. However, the barrier energy density for the initiation of a single STZ progressively increases with increasing Al content and the activation of shear transformation becomes less probable. Additionally, the broader distribution of STZs impedes their accumulation into large-sized flow units, leading to a lower number and reduced size of serrations in the load-displacement curves. On the contrary, the lower barrier energy densities in alloys containing only a small amount of Al enable a larger quantity of STZs to be activated simultaneously. These STZs are strongly localized and can easily percolate into large-sized flow units, which promote plastic flow through the formation and interaction of multiple shear bands. Employing the Poisson ratio as an indicator for plasticity, we have shown that this argumentation can be transferred to other types of metallic glasses. In principal, larger flow units were found for metallic glasses with higher Poisson ratio and more pronounced plasticity, while the flow units in alloys with very low Poisson ratio and high brittleness are significantly reduced in size and more homogeneously distributed throughout the material.

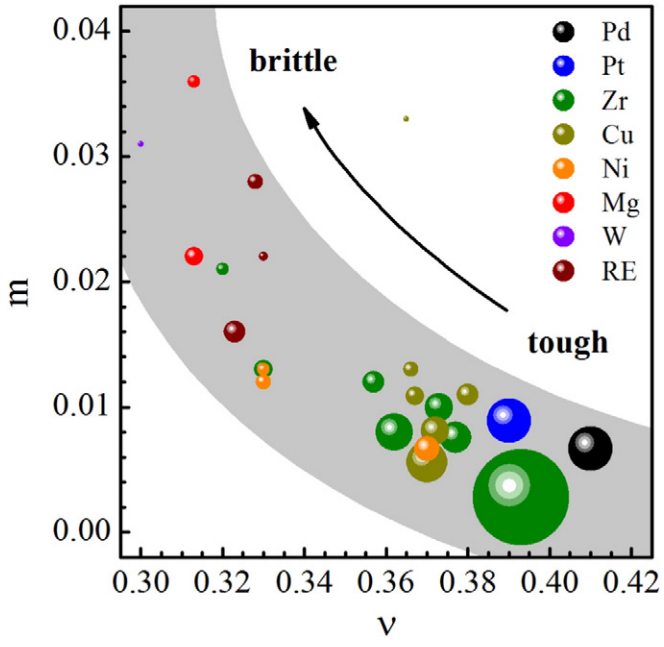

Fig. 8. Strain-rate sensitivity, m, of metallic glasses as a function of the Poisson ratio, ν. The graph includes experimental results on m from the current report and previous studies [15,18,22,27,48,62,99,100]. Poisson ratios of the ternary $(Cu_{0.5}Zr_{0.5})_{100-x}Al_x$ (x = 4, 5, 6 and 8 at.%) alloys and all other metallic glasses, for which no values of ν are given, were taken from Refs. [15,21,35,104–108]. The size of the symbols displays the number of atoms involved in the plastic flow events, N_{flow}, following the concept of Pan et al. [15], whereas the size differences in these flow units range from 149 ($Cu_{44}Zr_{44}Al_{12}$ [27]) to 2279 atoms ($Zr_{70}Ni_{16}Cu_6Al_8$ [22]).

Acknowledgement

Part of this work has been conducted within the priority program 1594 of the German Science Foundation (grants no. WO1220/8-1 and WO1220/10-1). Financial support is gratefully acknowledged.

References

[1] M.F. Ashby, A.L. Greer, Metallic glasses as structural materials, Scr. Mater. 54 (2006) 321–326.
[2] D.B. Miracle, A structural model for metallic glasses, Nat. Mater. 3 (2004) 697–702.
[3] H.W. Sheng, W.K. Luo, F.M. Alamgir, J.M. Bai, E. Ma, Atomic packing and short-to-medium-range order in metallic glasses, Nature 439 (2006) 419–425.
[4] A.L. Greer, Y.Q. Cheng, E. Ma, Shear bands in metallic glasses, Mater. Sci. Eng. R 74 (2013) 71–132.
[5] L. Wondraczek, J.C. Mauro, J. Eckert, U. Kühn, J. Horbach, J. Deubener, T. Rouxel, Towards ultrastrong glasses, Adv. Mater. 23 (2011) 4578–4586.
[6] A. Inoue, Stabilization of metallic supercooled liquid and bulk amorphous alloys, Acta Mater. 48 (2000) 279–306.
[7] W.H. Wang, Roles of minor additions in formation and properties of bulk metallic glasses, Prog. Mater. Sci. 52 (2007) 540–596.
[8] C.A. Schuh, T.C. Hufnagel, U. Ramamurty, Mechanical behavior of amorphous alloys, Acta Mater. 55 (2007) 4067–4109.
[9] M.W. Chen, Mechanical behavior of metallic glasses: microscopic understanding of strength and ductility, Annu. Rev. Mater. Res. 38 (2008) 445–469.
[10] M.M. Trexler, N.N. Thadhani, Mechanical properties of bulk metallic glasses, Prog. Mater. Sci. 55 (2010) 759–839.
[11] T.C. Hufnagel, C.A. Schuh, M.L. Falk, Deformation of metallic glasses: recent developments in theory, simulations, and experiments, Acta Mater. 109 (2016) 375–393.
[12] A.S. Argon, Plastic deformation in metallic glasses, Acta Metall. 27 (1979) 47–58.
[13] M.L. Falk, J.S. Langer, Dynamics of viscoplastic deformation in amorphous solids, Phys. Rev. E 57 (1998) 7192–7205.
[14] I.C. Choi, Y. Zhao, B.G. Yoo, Y.J. Kim, J.Y. Suh, U. Ramamurty, J.I. Jang, Estimation of the shear transformation zone size in a bulk metallic glass through statistical analysis of the first pop-in stresses during spherical nanoindentation, Scr. Mater. 66 (2012) 923–926.
[15] D. Pan, A. Inoue, T. Sakurai, M.W. Chen, Experimental characterization of shear transformation zones for plastic flow of bulk metallic glasses, P. Natl. Acad. Sci. USA 105 (2008) 14769–14772.
[16] W.L. Johnson, K. Samwer, A universal criterion for plastic yielding of metallic glasses with a $(T/T_g)^{2/3}$ temperature dependence, Phys. Rev. Lett. 95 (2005) 195501 (1–4).
[17] X. Qian, Q.P. Cao, S.Y. Liu, C. Wang, X.D. Wang, D.X. Zhang, U. Ramamurty, J.Z. Jiang, Dependence of shear yield strain and shear transformation zone on the glass transition temperature in thin film metallic glasses, J. Alloys Compd. 652 (2015) 191–199.
[18] Q.P. Cao, J.B. Jin, Y. Ma, X.Z. Cao, B.Y. Wang, S.X. Qu, X.D. Wang, D.X. Zhang, J.Z. Jiang, Enhanced plasticity in Zr-Cu-Ag-Al-Be bulk metallic glasses, J. Non-Cryst. Solids 412 (2015) 35–44.
[19] X.N. Zhao, Q.P. Cao, C. Wang, X.D. Wang, D.X. Zhang, S.X. Qu, J.Z. Jiang, Dependence of room-temperature nanoindentation creep behavior and shear transformation zone on the glass transition temperature in bulk metallic glasses, J. Non-Cryst. Solids 445–446 (2016) 19–29.

[20] L. Perrière, S. Nowak, S. Brossard, M.T. Thai, M. Blétry, Y. Champion, Nanoindentation study of chemical effects on the activation volume controlling shear band initiation in metallic glasses, Scr. Mater. 68 (2013) 183–186.
[21] Y. Ma, G.J. Peng, T.T. Debela, T.H. Zhang, Nanoindentation study on the characteristic of shear transformation zone volume in metallic glassy films, Scr. Mater. 108 (2015) 52–55.
[22] D. Pan, Y. Yokoyama, T. Fujita, Y.H. Liu, S. Kohara, A. Inoue, M.W. Chen, Correlation between structural relaxation and shear transformation zone volume of a bulk metallic glass, Appl. Phys. Lett. 95 (2009) 141909 (1–3).
[23] I.C. Choi, Y. Zhao, Y.J. Kim, B.G. Yoo, J.Y. Suh, U. Ramamurty, J.I. Jang, Indentation size effect and shear transformation zone size in a bulk metallic glass in two different structural states, Acta Mater. 60 (2012) 6862–6868.
[24] Y.K. Zhao, I.C. Choi, M.Y. Seok, M.H. Kim, D.H. Kim, U. Ramamurty, J.Y. Suh, J.I. Jang, Effect of hydrogen on the yielding behavior and shear transformation zone volume in metallic glass ribbons, Acta Mater. 78 (2014) 213–221.
[25] J.H. Perepezko, S.D. Imhoff, M.W. Chen, J.Q. Wang, S. Gonzalez, Nucleation of shear bands in amorphous alloys, Proc. Natl. Acad. Sci. U. S. A. 111 (2014) 3938–3942.
[26] W.D. Li, Y.F. Gao, H.B. Bei, On the correlation between microscopic structural heterogeneity and embrittlement behavior in metallic glasses, Sci. Rep. 5 (2015) 14786 (1–15).
[27] Y. Ma, J.H. Ye, G.J. Peng, D.H. Wen, T.H. Zhang, Loading rate effect on the creep behavior of metallic glassy films and its correlation with the shear transformation zone, Mater. Sci. Eng. A 622 (2015) 76–81.
[28] Y. Ma, G.J. Peng, Y.H. Feng, T.H. Zhang, Nanoindentation investigation on the creep mechanism in metallic glassy films, Mater. Sci. Eng. A 651 (2016) 548–555.
[29] P. Yu, H.Y. Bai, M.B. Tang, W.L. Wang, Excellent glass-forming ability in simple $Cu_{50}Zr_{50}$-based alloys, J. Non-Cryst. Solids 351 (2005) 1328–1332.
[30] T.L. Cheung, C.H. Shek, Thermal and mechanical properties of Cu-Zr-Al bulk metallic glasses, J. Alloys Compd. 434 (2007) 71–74.
[31] Q. Zhang, W. Zhang, G.Q. Xie, A. Inoue, Glass-forming ability and mechanical properties of the ternary Cu-Zr-Al and quaternary Cu-Zr-Al-Ag bulk metallic glasses, Mater. Trans. 48 (2007) 1626–1630.
[32] N.S. Barekar, S. Pauly, R.B. Kumar, U. Kuhn, B.K. Dhindaw, J. Eckert, Structure-property relations in bulk metallic Cu-Zr-Al alloys, Mater. Sci. Eng. A 527 (2010) 5867–5872.
[33] G. Kumar, T. Ohkubo, T. Mukai, K. Hono, Plasticity and microstructure of Zr-Cu-Al bulk metallic glasses, Scr. Mater. 57 (2007) 173–176.
[34] T.A. Baser, J. Das, J. Eckert, M. Baricco, Glass formation and mechanical properties of $(Cu_{50}Zr_{50})_{100-x}Al_x$ (x = 0, 4, 5, 7) bulk metallic glasses, J. Alloys Compd. 483 (2009) 146–149.
[35] P. Yu, H.Y. Bai, Poisson's ratio and plasticity in CuZrAl bulk metallic glasses, Mater. Sci. Eng. A 485 (2008) 1–4.
[36] S. Pauly, S. Gorantla, G. Wang, U. Kuhn, J. Eckert, Transformation-mediated ductility in CuZr-based bulk metallic glasses, Nat. Mater. 9 (2010) 473–477.
[37] R. Limbach, B.P. Rodrigues, L. Wondraczek, Strain-rate sensitivity of glasses, J. Non-Cryst. Solids 404 (2014) 124–134.
[38] W.C. Oliver, G.M. Pharr, An improved technique for determining hardness and elastic modulus using load and displacement sensing indentation experiments, J. Mater. Res. 7 (1992) 1564–1583.
[39] J. Hay, Introduction to instrumented indentation testing, Exp. Tech. 33 (2009) 66–72.
[40] P. Yu, H.Y. Bai, W.H. Wang, Superior glass-forming ability of CuZr alloys from minor additions, J. Mater. Res. 21 (2006) 1674–1679.
[41] X.D. Wang, Q.K. Jiang, Q.P. Cao, J. Bednarcik, H. Franz, J.Z. Jiang, Atomic structure and glass forming ability of $Cu_{46}Zr_{46}Al_8$ bulk metallic glass, J. Appl. Phys. 104 (2008) 093519 (1–5).
[42] W.H. Wang, J.J. Lewandowski, A.L. Greer, Understanding the glass-forming ability of $Cu_{50}Zr_{50}$ alloys in terms of a metastable eutectic, J. Mater. Res. 20 (2005) 2307–2313.
[43] W.D. Nix, H.J. Gao, Indentation size effects in crystalline materials: a law for strain gradient plasticity, J. Mech. Phys. Solids 46 (1998) 411–425.
[44] N. Van Steenberge, J. Sort, A. Concustell, J. Das, S. Scudino, S. Surinach, J. Eckert, M.D. Baro, Dynamic softening and indentation size effect in a Zr-based bulk glass-forming alloy, Scr. Mater. 56 (2007) 605–608.
[45] N. Li, K.C. Chan, L. Liu, The indentation size effect in $Pd_{40}Cu_{30}Ni_{10}P_{20}$ bulk metallic glass, J. Phys. D. Appl. Phys. 41 (2008) 155415 (1–5).
[46] Y.J. Huang, J. Shen, Y. Sun, J.F. Sun, Indentation size effect of hardness of metallic glasses, Mater. Des. 31 (2010) 1563–1566.
[47] J.I. Jang, B.G. Yoo, Y.J. Kim, J.H. Oh, I.C. Choi, H.B. Bei, Indentation size effect in bulk metallic glass, Scr. Mater. 64 (2011) 753–756.
[48] L. Cheng, Z.M. Jiao, S.G. Ma, J.W. Qiao, Z.H. Wang, Serrated flow behaviors of a Zr-based bulk metallic glass by nanoindentation, J. Appl. Phys. 115 (2014) 084907 (1–5).
[49] F. Xu, Y.H. Ding, X.H. Deng, P. Zhang, Z.L. Long, Indentation size effects in the nano- and micro-hardness of a Fe-based bulk metallic glass, Physica B 450 (2014) 84–89.
[50] F. Xue, F. Wang, P. Huang, T.J. Lu, K.W. Xu, Structural inhomogeneity and strain rate dependent indentation size effect in Zr-based metallic glass, Mater. Sci. Eng. A 655 (2016) 373–378.
[51] F. Spaepen, Microscopic mechanism for steady-state inhomogeneous flow in metallic glasses, Acta Metall. 25 (1977) 407–415.
[52] W.H. Wang, Elastic moduli and behaviors of metallic glasses, J. Non-Cryst. Solids 351 (2005) 1481–1485.
[53] W.H. Wang, Correlations between elastic moduli and properties in bulk metallic glasses, J. Appl. Phys. 99 (2006) 093506 (1−10).
[54] T. Rouxel, Y. Yokoyama, Elastic properties and atomic bonding character in metallic glasses, J. Appl. Phys. 118 (2015) 044901 (1–6).
[55] C.E. Lekka, G.A. Evangelakis, Bonding characteristics and strengthening of CuZr fundamental clusters upon small Al additions from density functional theory calculations, Scr. Mater. 61 (2009) 974–977.
[56] Y.Q. Cheng, E. Ma, Atomic-level structure and structure-property relationship in metallic glasses, Prog. Mater. Sci. 56 (2011) 379–473.
[57] W.H. Wang, The elastic properties, elastic models and elastic perspectives of metallic glasses, Prog. Mater. Sci. 57 (2012) 487–656.
[58] A. Concustell, J. Sort, G. Alcala, S. Mato, A. Gebert, J. Eckert, M.D. Baro, Plastic deformation and mechanical softening of $Pd_{40}Cu_{30}Ni_{10}P_{20}$ bulk metallic glass during nanoindentation, J. Mater. Res. 20 (2005) 2719–2725.
[59] Y.H. Lee, J.Y. Kim, S.H. Nahm, D. Kwon, Loading rate effect on inelastic deformation in a Zr-based bulk metallic glass, Mater. Sci. Eng. A 449 (2007) 185–188.
[60] B.C. Wei, L.C. Zhang, T.H. Zhang, D.M. Xing, J. Das, J. Eckert, Strain rate dependence of plastic flow in Ce-based bulk metallic glass during nanoindentation, J. Mater. Res. 22 (2007) 258–263.
[61] L.C. Zhang, B.C. Wei, D.M. Xing, T.H. Zhang, W.H. Li, Y. Liu, The characterization of plastic deformation in Ce-based bulk metallic glasses, Intermetallics 15 (2007) 791–795.
[62] D. Pan, M.W. Chen, Rate-change instrumented indentation for measuring strain rate sensitivity, J. Mater. Res. 24 (2009) 1466–1470.
[63] J.J. Pang, M.J. Tan, K.M. Liew, C. Shearwood, Nanoindentation study of size effect and loading rate effect on mechanical properties of a thin film metallic glass $Cu_{49.3}Zr_{50.7}$, Physica B 407 (2012) 340–346.
[64] J. Sort, J. Fornell, W. Li, S. Surinach, M.D. Baro, Influence of the loading rate on the indentation response of Ti-based metallic glass, J. Mater. Res. 24 (2009) 918–925.
[65] A. Bhattacharyya, G. Singh, K.E. Prasad, R. Narasimhan, U. Ramamurty, On the strain rate sensitivity of plastic flow in metallic glasses, Mater. Sci. Eng. A 625 (2015) 245–251.
[66] Y.I. Golovin, V.I. Ivolgin, V.A. Khonik, K. Kitagawa, A.I. Tyurin, Serrated plastic flow during nanoindentation of a bulk metallic glass, Scr. Mater. 45 (2001) 947–952.
[67] C.A. Schuh, T.G. Nieh, A nanoindentation study of serrated flow in bulk metallic glasses, Acta Mater. 51 (2003) 87–99.
[68] C.A. Schuh, T.G. Nieh, Y. Kawamura, Rate dependence of serrated flow during nanoindentation of a bulk metallic glass, J. Mater. Res. 17 (2002) 1651–1654.
[69] L. Liu, K.C. Chan, Plastic deformation of Zr-based bulk metallic glasses under nanoindentation, Mater. Lett. 59 (2005) 3090–3094.
[70] B. Yang, T.G. Nieh, Effect of the nanoindentation rate on the shear band formation in an Au-based bulk metallic glass, Acta Mater. 55 (2007) 295–300.
[71] T. Burgess, K.J. Laws, M. Ferry, Effect of loading rate on the serrated flow of a bulk metallic glass during nanoindentation, Acta Mater. 56 (2008) 4829–4835.
[72] K.Y. Ng, L. Zuo, A.H.W. Ngan, Steady-state serrated deformation of metallic glass during indentation, Scr. Mater. 61 (2009) 955–958.
[73] B.G. Yoo, K.W. Lee, J.I. Jang, Instrumented indentation of a Pd-based bulk metallic glass: constant loading-rate test vs constant strain-rate test, J. Alloys Compd. 483 (2009) 136–138.
[74] B.N. Lucas, W.C. Oliver, Indentation power-law creep of high-purity indium, Metall. Mater. Trans. A 30 (1999) 601–610.
[75] X.H. Lin, W.L. Johnson, W.K. Rhim, Effect of oxygen impurity on crystallization of an undercooled bulk glass forming Zr-Ti-Cu-Ni-Al alloy, Mater. Trans. JIM 38 (1997) 473–477.
[76] Y.J. Huang, J. Shen, Y.L. Chiu, J.J.J. Chen, J.F. Sun, Indentation creep of an Fe-based bulk metallic glass, Intermetallics 17 (2009) 190–194.
[77] F. Xu, Z.L. Long, X.H. Deng, P. Zhang, Loading rate sensitivity of nanoindentation creep behavior in a Fe-based bulk metallic glass, Trans. Nonferrous Metals Soc. China 23 (2013) 1646–1651.
[78] Y. Ma, J.H. Ye, G.J. Peng, D.H. Wen, T.H. Zhang, Nanoindentation study of size effect on shear transformation zone size in a Ni-Nb metallic glass, Mater. Sci. Eng. A 627 (2015) 153–160.
[79] L.Y. Chen, Z.D. Fu, G.Q. Zhang, X.P. Hao, Q.K. Jiang, X.D. Wang, Q.P. Cao, H. Franz, Y.G. Liu, H.S. Xie, S.L. Zhang, B.Y. Wang, Y.W. Zeng, J.Z. Jiang, New class of plastic bulk metallic glass, Phys. Rev. Lett. 100 (2008) 075501 (1–4).
[80] J. Pan, L. Liu, K.C. Chan, Enhanced plasticity by phase separation in CuZrAl bulk metallic glass with micro-addition of Fe, Scr. Mater. 60 (2009) 822–825.
[81] J. Pan, K.C. Chan, Q. Chen, N. Li, S.F. Guo, L. Liu, The effect of microalloying on mechanical properties in CuZrAl bulk metallic glass, J. Alloys Compd. 504 (2010) S74–S77.
[82] W. Zhou, J.X. Hou, W.P. Weng, Microstructure, thermal stability and mechanical properties of Zr-Cu-Al-Sn bulk metallic glass, J. Non-Cryst. Solids 429 (2015) 208–212.
[83] S. Scudino, B. Jerliu, K.B. Surreddi, U. Kuhn, J. Eckert, Effect of cold rolling on compressive and tensile mechanical properties of $Zr_{52.5}Ti_5Cu_{18}Ni_{14.5}Al_{10}$ bulk metallic glass, J. Alloys Compd. 509 (2011) S128–S130.
[84] C.A. Schuh, A.C. Lund, T.G. Nieh, New regime of homogeneous flow in the deformation map of metallic glasses: elevated temperature nanoindentation experiments and mechanistic modeling, Acta Mater. 52 (2004) 5879–5891.
[85] W.H. Li, T.H. Zhang, D.M. Xing, B.C. Wei, Y.R. Wang, Y.D. Dong, Instrumented indentation study of plastic deformation in bulk metallic glasses, J. Mater. Res. 21 (2006) 75–81.
[86] W.H. Li, B.C. Wei, T.H. Zhang, D.M. Xing, L.C. Zhang, Y.R. Wang, Study of serrated flow and plastic deformation in metallic glasses through instrumented indentation, Intermetallics 15 (2007) 706–710.
[87] T.G. Nieh, C. Schuh, J. Wadsworth, Y. Li, Strain rate-dependent deformation in bulk metallic glasses, Intermetallics 10 (2002) 1177–1182.
[88] C.A. Schuh, T.G. Nieh, A survey of instrumented indentation studies on metallic glasses, J. Mater. Res. 19 (2004) 46–57.

[89] J.I. Jang, B.G. Yoo, J.Y. Kim, Rate-dependent inhomogeneous-to-homogeneous transition of plastic flows during nanoindentation of bulk metallic glasses: fact or artifact? Appl. Phys. Lett. 90 (2007) 211906 (1–3).
[90] H. Bei, Z.P. Lu, E.P. George, Theoretical strength and the onset of plasticity in bulk metallic glasses investigated by nanoindentation with a spherical indenter, Phys. Rev. Lett. 93 (2004) 125504 (1–4).
[91] K.L. Johnson, Contact Mechanics, Cambridge University Press, Cambridge, UK, 1985.
[92] C.E. Packard, O. Franke, E.R. Homer, C.A. Schuh, Nanoscale strength distribution in amorphous versus crystalline metals, J. Mater. Res. 25 (2010) 2251–2263.
[93] D. Tönnies, K. Samwer, P.M. Derlet, C.A. Volkert, R. Maass, Rate-dependent shear-band initiation in a metallic glass, Appl. Phys. Lett. 106 (2015) 171907 (1–4).
[94] C.A. Schuh, A.C. Lund, Application of nucleation theory to the rate dependence of incipient plasticity during nanoindentation, J. Mater. Res. 19 (2004) 2152–2158.
[95] F. Jiang, M.Q. Jiang, H.F. Wang, Y.L. Zhao, L. He, J. Sun, Shear transformation zone volume determining ductile-brittle transition of bulk metallic glasses, Acta Mater. 59 (2011) 2057–2068.
[96] J.J. Lewandowski, W.H. Wang, A.L. Greer, Intrinsic plasticity or brittleness of metallic glasses, Philos. Mag. Lett. 85 (2005) 77–87.
[97] S.T. Liu, Z. Wang, H.L. Peng, H.B. Yu, W.H. Wang, The activation energy and volume of flow units of metallic glasses, Scr. Mater. 67 (2012) 9–12.
[98] D. Tabor, The hardness of solids, Rev. Phys. Technol. 1 (1970) 145–179.
[99] Y.D. Sun, Z.Q. Li, J.S. Liu, M.Q. Cong, J.Y. Qin, Indentation creep behaviors of $Mg_{61}Cu_{28}Gd_{11}$ and $(Mg_{61}Cu_{28}Gd_{11})_{99.5}Sb_{0.5}$ bulk metallic glasses at room temperature, J. Rare Earths 29 (2011) 253–258.
[100] B.C. Wei, T.H. Zhang, W.H. Li, D.M. Xing, L.C. Zhang, Y.R. Wang, Indentation creep behavior in Ce-based bulk metallic glasses at room temperature, Mater. Trans. 46 (2005) 2959–2962.
[101] F. Wang, J.M. Li, P. Huang, W.L. Wang, T.J. Lu, K.W. Xu, Nanoscale creep deformation in Zr-based metallic glass, Intermetallics 38 (2013) 156–160.
[102] F.C. Li, Y. Xie, M. Song, S. Ni, S.F. Guo, X.Z. Liao, A detailed appraisal of the stress exponent used for characterizing creep behavior in metallic glasses, Mater. Sci. Eng. A 654 (2016) 53–59.
[103] Y.H. Liu, K. Wang, A. Inoue, T. Sakurai, M.W. Chen, Energetic criterion on the intrinsic ductility of bulk metallic glasses, Scr. Mater. 62 (2010) 586–589.
[104] X.K. Xi, R.J. Wang, D.Q. Zhao, M.X. Pan, W.H. Wang, Glass-forming Mg-Cu-RE (RE = Gd, Pr, Nd, Tb, Y, and Dy) alloys with strong oxygen resistance in manufacturability, J. Non-Cryst. Solids 344 (2004) 105–109.
[105] B. Zhang, D.Q. Zhao, M. Pan, R.J. Wang, W.H. Wang, Formation of cerium-based bulk metallic glasses, Acta Mater. 54 (2006) 3025–3032.
[106] Z.Y. Zhang, V. Keppens, P.K. Liaw, Y. Yokoyama, A. Inoue, Elastic properties of Zr-based bulk metallic glasses studied by resonant ultrasound spectroscopy, J. Mater. Res. 22 (2007) 364–367.
[107] J. Fornell, S. Surinach, M.D. Baro, J. Sort, Unconventional elastic properties, deformation behavior and fracture characteristics of newly developed rare earth bulk metallic glasses, Intermetallics 17 (2009) 1090–1097.
[108] Y. Yokoyama, K. Fujita, A.R. Yavari, A. Inoue, Malleable hypoeutectic Zr-Ni-Cu-Al bulk glassy alloys with tensile plastic elongation at room temperature, Philos. Mag. Lett. 89 (2009) 322–334.